Main Manuscript for

Comparative Analysis of AAV Serotypes for Transduction of Olfactory Sensory Neurons

Benjamin D.W. Belfort*[1,2,3,4,5], Johnathan D. Jia*[3,5,6], Alexandra Garza^[1,2,3,5], Anthony M. Insalaco^[2,3], JP McGinnis[3,7], Brandon T. Pekarek[1,2,3], Joshua Ortiz-Guzman[3], Burak Tepe[2,3], Hu Chen[3,5,6], Zhandong Liu[3,5,6], Benjamin R. Arenkiel°[,2,3,5,8]

1 Genetics and Genomics Graduate Program, Baylor College of Medicine, Houston, Texas 77030, USA.
2 Department of Molecular and Human Genetics, Baylor College of Medicine, Houston, Texas 77030, USA.
3 Jan and Dan Duncan Neurological Research Institute, Texas Children's Hospital, Houston, Texas 77030, USA
4 Medical Scientist Training Program, Baylor College of Medicine, Houston, Texas 77030, USA.
5 Aligning Science Across Parkinson's (ASAP) Collaborative Research Network, Chevy Chase, MD 20815.
6 Department of Pediatrics, Section of Neurology, Baylor College of Medicine, Houston, Texas 77030, USA
7 Department of Neurosurgery, Baylor College of Medicine, Houston, Texas 77030, USA
8 Department of Neuroscience, Baylor College of Medicine, Houston, Texas 77030, USA.
*,^ These authors contributed equally

° Corresponding author: Benjamin R. Arenkiel

Email: Arenkiel@bcm.edu

Author Contributions: BDWB and BRA- project conceptualization; JJ and BDWB- bioinformatic analyses; BDWB, AG, AMI- performed research; JPM, JOG- provided essential resources; BDWB, JJ, AG, AMI- performed analyses; BDWB, JJ- wrote the paper; BP, BT, HC- provided feedback and technical support.

Competing Interest Statement: Disclose any competing interests here.

Classification: Neuroscience

Keywords: AAV, gene therapy, olfaction, olfactory sensory neurons

This file includes:

Main Text
Figures 1 to 2
Table 1

Abstract

Olfactory sensory neurons within the nasal epithelium detect volatile odorants and relay odor information to the central nervous system. Unlike other sensory inputs, olfactory sensory neurons interface with the external environment and project their axons directly into the central nervous system. The use of adeno-associated viruses to target these neurons has garnered interest for applications in gene therapy, probing olfactory sensory neuron biology, and modeling disease. To date, there is no consensus on the optimal AAV serotype for efficient and selective transduction of olfactory sensory neurons *in vivo*. Here we utilized serial confocal imaging and single-nucleus RNA sequencing to evaluate the efficacy of 11 different AAV serotypes in transducing murine olfactory sensory neurons via non-invasive nasal inoculation. Our results reveal that AAV1, while highly effective, exhibited broad tropism, whereas AAV-DJ/8 showed the greatest specificity for olfactory sensory neurons.

Main Text

Introduction

The mammalian olfactory epithelium (OE) is a specialized epithelial tissue within the nose that plays a critical role in the sense of smell. Olfactory sensory neurons (OSNs) are specialized chemosensory neurons that reside in the OE and detect airborne chemicals through G-protein coupled odorant receptors. OSNs project their axons directly into the olfactory bulb (OB), creating a single-neuron chain between the external environment and the central nervous system (CNS). This conduit into the CNS provides unique opportunities for probing OSN biology, administering targeted gene therapies, and modeling disease. The use of AAVs has been explored for these purposes [1], yet information is lacking on the optimal serotype for transducing OSNs. In the present study, we leveraged confocal imaging and single-nucleus RNA sequencing (snRNAseq) to identify optimal AAV serotypes for *in vivo* transduction of murine OSNs.

Results

To test the efficacy of AAV transduction across commonly used serotypes, we packaged an identical construct (rAAV-EF1a-TdTomato-WPRE-PolyA) into 11 different AAV capsid serotypes with reported OE and neuronal transduction[1]. Serotypes included AAV1, AAV2, AAV5, AAV7, AAV8, AAV9, AAV-DJ/8[2,3], AAV-PhP.eB [4], AAV-PhP.S [4], AAV-rh10 [5,6], and AAV-SCH9 [7]. Each AAV serotype was introduced via non-invasive nasal inoculation (NINI) [8] into three male mice per serotype, for a total of 33 experimental animals. After a four-week expression period, the OB was processed to quantify colocalized olfactory marker protein (OMP) and TdTomato expression within OSN axon terminals as a readout for the number of transduced OSNs [Fig. 1A]. By first focusing on the reporter expression in the glomerular layer of the OB, we avoided potentially confounding TdTomato signals from other transduced accessory cell types within the OE [Fig. 1B].

For quantification, we performed confocal image analysis across OSN terminal fields within the glomerular layer via immunostaining, measuring levels of tdTomato reporter expression alongside OMP. Importantly, we found no difference in total OMP area between samples from each serotype [Fig. 1C], suggesting that transduction itself did not compromise overall OSN viability or OE integrity. We next quantified the amount of TdTomato surface area (normalized to OMP surface area) per section, and found that AAV1, AAV7, AAV-DJ/8, and AAV-rh10 displayed the greatest levels of expression [Fig. 1D] in OSN terminals that project to the olfactory bulb.

Following this primary reporter expression screen, we next performed snRNAseq to more accurately quantify OSN transduction efficiency of the top 4 candidates in the different OE cell types. Towards this, we designed 4 new AAV expression constructs, all identical aside from a short barcode sequence (“ID”) that identifies the corresponding AAV serotype upon transduction and snRNA sequencing. The 4 AAVs were mixed at equal titer and introduced into wildtype mice via NINI. After 4 weeks of *in vivo* expression, OE was harvested for snRNAseq [Fig. 2A]. Data were processed following standard scRNAseq guidelines [9]. Using 20,081 high-quality nuclei, we generated an annotated UMAP from known cell type-specific markers (see SI appendix) to quantify the distribution of cell types [Fig. 2B-D] and identify those that were differentially transduced by the four candidate AAV serotypes. We confirmed cell type lineages by comparing terminal fate probabilities from Palantir pseudotime analysis, with Horizontal Basal Cells

(HBCs) designated as the starting point and mature OSN (mOSN), mature sustentacular (mSus), microvillar (MVC), and Bowman's gland (BowG) cells as terminal fates [10] [Fig. E-F]. A 2-sided t-test (α = 0.05) and chi-squared goodness of fit indicated that the terminal fate probabilities between GBCs and iSus cells were different for mOSN and mSus lineages [Fig. 2G]. Finally, we quantified the number and type of cells that were effectively transduced for each AAV serotype [Fig. 2H]. In total, we identified 382 cells that harbored AAV barcodes. While mature OSN (mOSN) transduction efficiency was highest for AAV1 [Fig. 2I], AAV-DJ/8 showed the greatest specificity for mOSNs [Fig. 2J]. Further examination of AAV1 expression showed broad tropism, with immature sustentacular (iSus) and airway ciliated cells (ACCs) contributing to the highest normalized cell counts [Fig. 2K].

Discussion

In the present study, we leveraged confocal imaging and snRNAseq to identify optimal AAV serotypes for *in vivo* OSN transduction via NINI. Despite variability in our imaging dataset, attributable to unpredictable flow of fluid through the nasal turbinates during NINI, AAV1, AAV7, AAV-DJ/8, and AAV-rh10 displayed the greatest efficacy in their ability to transduce OSNs compared to other AAV serotypes we tested [Fig. 1D]. To determine which serotype was most efficient at transducing OSNs in a more quantitative, higher-resolution, and cell type-specific manner, we employed snRNA sequencing from isolated OE. Though this is the first study to employ snRNAseq of the OE, we found that clustering and cell type distribution were similar to other single-cell sequencing studies previously performed on the OE[11,12] [Fig. 2B-D]. We found that cell subsets comprised known lineages of interest, namely HBCs, globose basal cells (GBCs), iOSNs, mOSNs, iSus, mSus, MVCs, and BowGs, and determined the corresponding pseudotemporal lineage patterns [Fig. 2E]. Through this, we substantiated cell type identities by comparing their terminal fate probabilities. Of interest, the terminal fate probability distribution of HBCs properly reflected multiple cell types, indicating their pluripotent ability to divide into all lineages of interest, but favoring mOSNs, mSus, and MVCs [Fig. 2F]. By comparing the terminal fates of iSus and GBC, we further validated the identified OSN and sustentacular cell lineages. Having confirmed the cellular composition of the transduced tissue, we next quantified the number of AAV+ cells within each cell type cluster [Fig. 2H]. Of the serotypes tested, AAV1 showed the highest transduction efficiency of OSNs [Fig. 2I], but AAV-DJ/8, AAV7, and AAV-rh10 all showed greater OSN specificity, with AAV-DJ/8 showing the greatest specificity compared to AAV1 [Fig. 2J]. From these data, we also found that AAV1 showed the broadest tropism in the OE; transducing cell types such as HBCs, GBCs, ACCs, and particularly iSus, all with greater efficiency than OSNs [Fig. 2K and Table 1]. Alongside a census of the cell types that comprise the mouse olfactory epithelium, together these findings also present useful implications for future research, including OSN-targeted gene therapy, probing OSN biology, modeling diseases where the OE and OB are loci of interest (e.g., Parkinson's disease and Alzheimer's disease), and informing the development of future AAV capsids for targeting OSNs.

Materials and Methods

All mice used in this study were male C57BL/6J (Jax :000664), and all experimentation was performed in compliance with Baylor College of Medicine IACUC. For extended materials and methods, see SI Appendix.

Acknowledgments

This research was funded in whole or in part by Aligning Science Across Parkinson's [10000400] through the Michael J. Fox Foundation for Parkinson's Research (MJFF). For the purpose of open access, the author has applied a CC BY public copyright license to all Author Accepted Manuscripts arising from this submission. Special thanks to the Texas Children's Hospital Neuroconnectivity Core for assistance with viral packaging and Baylor College of Medicine's Single Cell Genomics Core for assistance with snRNAseq library preparation.

References

1. Gadenstaetter AJ, Schmutzler L, Grimm D, Landegger LD. Intranasal application of adeno-associated viruses: a systematic review. Translational Research. 2022;248:87-110. doi:10.1016/j.trsl.2022.05.002
2. Grimm D, Lee JS, Wang L, et al. In Vitro and In Vivo Gene Therapy Vector Evolution via Multispecies Interbreeding and Retargeting of Adeno-Associated Viruses. J Virol. 2008;82(12):5887-5911. doi:10.1128/jvi.00254-08
3. Hammond SL, Leek AN, Richman EH, Tjalkens RB. Cellular selectivity of AAV serotypes for gene delivery in neurons and astrocytes by neonatal intracerebroventricular injection. PLoS One. 2017;12(12). doi:10.1371/journal.pone.0188830
4. Chan KY, Jang MJ, Yoo BB, et al. Engineered AAVs for efficient noninvasive gene delivery to the central and peripheral nervous systems. Nat Neurosci. 2017;20(8):1172-1179. doi:10.1038/nn.4593
5. Cearley CN, Wolfe JH. Transduction characteristics of adeno-associated virus vectors expressing cap serotypes 7, 8, 9, and Rh10 in the mouse brain. Molecular Therapy. 2006;13(3):528-537. doi:10.1016/j.ymthe.2005.11.015
6. Gao GP, Alvira MR, Wang L, Calcedo R, Johnston J, Wilson JM. Novel Adeno-Associated Viruses from Rhesus Monkeys as Vectors for Human Gene Therapy. www.pnas.orgcgidoi10.1073pnas.182412299
7. Ojala DS, Sun S, Santiago-Ortiz JL, Shapiro MG, Romero PA, Schaffer D V. In Vivo Selection of a Computationally Designed SCHEMA AAV Library Yields a Novel Variant for Infection of Adult Neural Stem Cells in the SVZ. *Molecular Therapy*. 2018;26(1):304-319. doi:10.1016/j.ymthe.2017.09.006
8. Santry LA, Ingrao JC, Yu DL, et al. AAV vector distribution in the mouse respiratory tract following four different methods of administration. BMC Biotechnol. 2017;17(1). doi:10.1186/s12896-017-0365-2
9. Wolf FA, Angerer P, Theis FJ. SCANPY: Large-scale single-cell gene expression data analysis. Genome Biol. 2018;19(1). doi:10.1186/s13059-017-1382-0
10. Setty M, Kiseliovas V, Levine J, Gayoso A, Mazutis L, Pe'er D. Characterization of cell fate probabilities in single-cell data with Palantir. Nat Biotechnol. 2019;37(4):451-460. doi:10.1038/s41587-019-0068-4
11. Brann DH, Tsukahara T, Weinreb C, Lipovsek M, Van den Berge K, Gong B, Chance R, Macaulay IC, Chou HJ, Fletcher RB, Das D, Street K, de Bezieux HR, Choi YG, Risso D, Dudoit S, Purdom E, Mill J, Hachem RA, Matsunami H, Logan DW, Goldstein BJ, Grubb MS, Ngai J, Datta SR. Non-neuronal expression of SARS-CoV-2 entry genes in the olfactory system suggests mechanisms underlying COVID-19-associated anosmia. Sci Adv. 2020 Jul 31;6(31):eabc5801. doi: 10.1126/sciadv.abc5801.
12. Fletcher RB, Das D, Gadye L, et al. Deconstructing Olfactory Stem Cell Trajectories at Single-Cell Resolution. Cell Stem Cell. 2017;20(6):817-830.e8. doi:10.1016/j.stem.2017.04.003

Figures

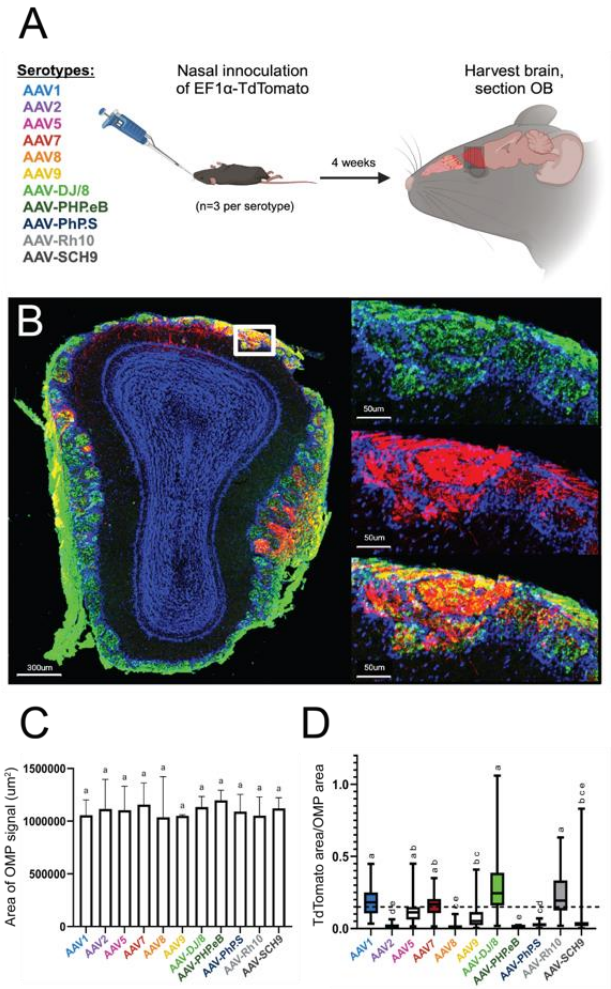

Figure 1. Confocal imaging identifies AAV1, AAV7, AAV-DJ/8, and AAV-rh10 as efficient AAV serotypes for OSN transduction. A) Overview of experimental paradigm. B) Representative confocal image of OB cross-section from AAV1 inoculated mouse. Upper right: close-up of OSNs forming the structures of the glomerular and olfactory nerve layers of the OB, with OMP (green) channel isolated. Middle right: close-up of the same region, with TdTomato (red) channel isolated. Bottom right: overlay of OMP and TdTomato channels. Blue= Hoechst. C) Total area of OMP signal per OB for each serotype. D) Quantification of the percentage of TdTomato/OMP per OB section. Results of one-way ANOVA are represented by compact letter display.

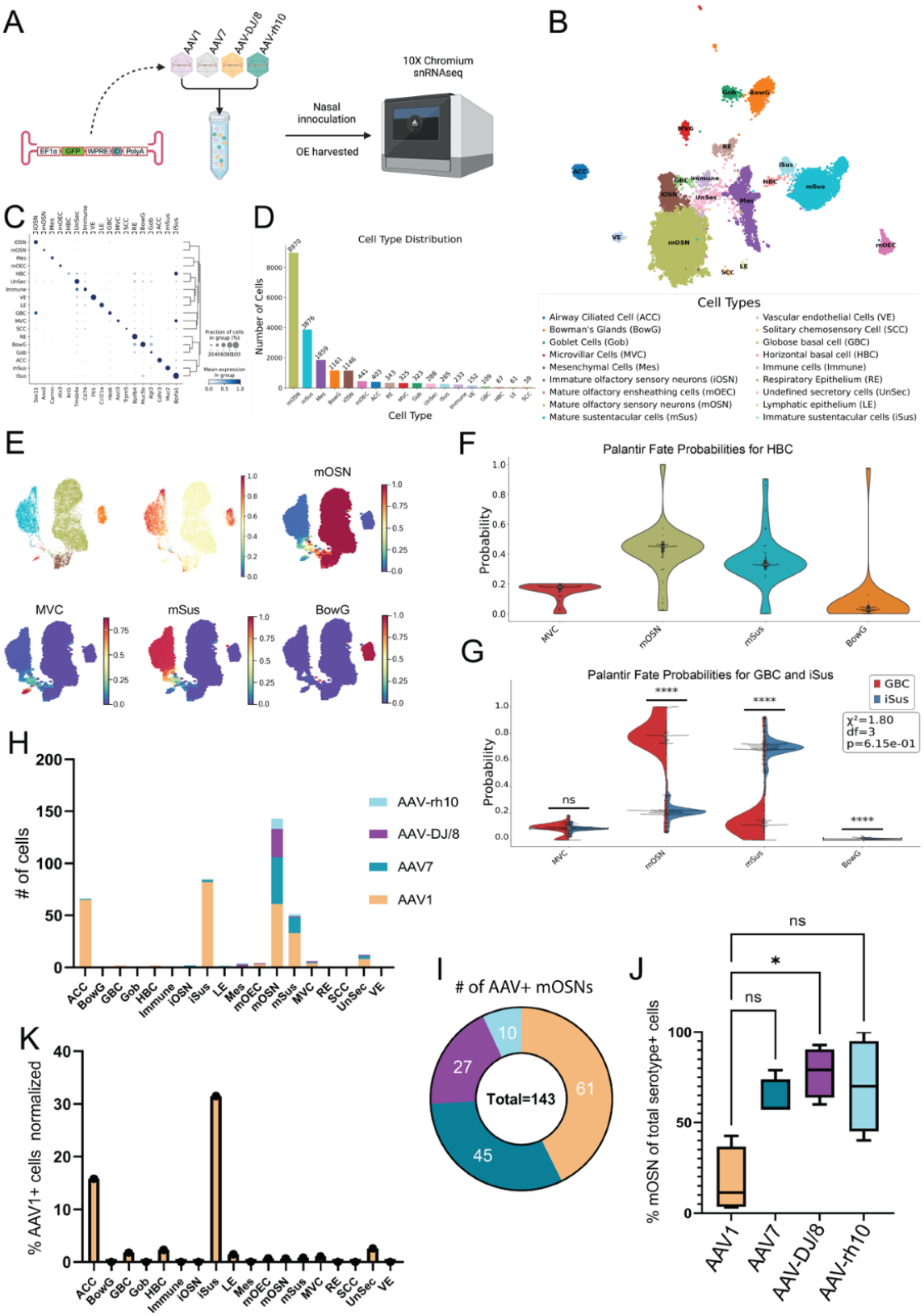

Figure 2. Single nucleus transcriptomics shows AAV1 has the greatest transduction rate while AAV-DJ/8 has the greatest specificity for mOSNs. A) Experimental workflow. B) UMAP of snRNAseq dataset. C) Dot plot showing the cell-type specific markers used for annotations. The x-axis is the marker,

and the y-axis is the cell type. D) Cell type distribution with total cell counts. The x-axis is the cell type with each bar's color reflecting the corresponding color on the UMAP, and the y-axis is the absolute count of the respective cell types. E) Minimum distortion embedding (MDE) with our specific lineages of interest including mOSN, mSus, MVC, and BowG lineages. The total OE cell type-specific pseudotime is shown above and individual lineage pseudotimes shown below, with red indicating late pseudotime and dark blue indicating early pseudotime. F) Violin-box plot of terminal fate probability of HBCs calculated from the Palantir pseudotime. G) Terminal fate probabilities of GBCs and iSus were compared using a 2-sided t-test ($\alpha = 0.05$) and chi-squared goodness of fit for each possible terminal fate. The stars represent the level of significance. For $p < 1e^{-4}$ there are 4 stars, $< 1e^{-3}$ are 3 stars, 2 stars for < 0.01, 1 star for < 0.05, and ns for not significant. Chi-squared GOF was used to evaluate overall differences between terminal fate probabilities of each cluster. H) Total AAV+ cell counts per cell type. I) Total AAV+ mOSN cell counts. J) Percent of total serotype positive cells which are mOSNs. * $p < .05$, Kruskal-Wallis test. K) Percent AAV1+ cell counts of each cell type cluster total cell count.